Journal of Magnetic Resonance 210 (2011) 1–6

Contents lists available at ScienceDirect

Journal of Magnetic Resonance

journal homepage: www.elsevier.com/locate/jmr

NMR signal averaging in 62 T pulsed fields

Benno Meier [a], Sebastian Greiser [a], Jürgen Haase [a,*], Thomas Herrmannsdörfer [b], Frederik Wolff-Fabris [b], Jochen Wosnitza [b]

[a] University of Leipzig, Faculty of Physics and Earth Science, Linnéstrasse 5, 04103 Leipzig, Germany
[b] Hochfeld-Magnetlabor Dresden, Forschungszentrum Dresden-Rossendorf, 01314 Dresden, Germany

ARTICLE INFO

Article history:
Received 8 December 2010
Revised 28 January 2011
Available online 1 March 2011

Keywords:
NMR
Pulsed magnetic fields

ABSTRACT

Nuclear Magnetic Resonance (NMR) experiments in pulsed high magnetic fields up to 62 T at the Dresden High Magnetic Field Laboratory (*Hochfeld-Magnetlabor Dresden*) are reported. The time dependence of the magnetic field is investigated by observing various free induction decays (FIDs) in the vicinity of the maximum of the field pulse. By analyzing each FID's phase and its evolution with time the magnetic field's time dependence can be determined with high precision. Assuming a quadratic or cubic dependence on time near the field maximum its confidence is found to be better than ±0.03 ppm at low fields and ±0.8 ppm near 62 T. In turn, the thus obtained time dependence of the field can be used to demodulate and phase-correct all FIDs so that they appear phase-locked to each other. As a consequence signal averaging is possible. The increase in signal-to-noise ratio is found to be close to that expected theoretically. This shows that the intrinsic time dependence of the pulsed fields can be removed so that the NMR signals appear to be taken at rather stable static field. This opens up the possibility of performing precise shift measurements and signal averaging also of unknown, weak signals if a reference signal is measured during the same field pulse with a double-resonance probe.

1. Introduction

Sensitivity and resolution are central to most NMR experiments. That is the reason why high magnetic fields are of great interest provided they come with sufficient spatial homogeneity and temporal stability. Of course, the concrete requirements depend on the particular experiment, and for the investigation of solids with large linewidths the requirements are less stringent. In fact, for many applications of NMR in the area of modern condensed matter physics, in particular for the investigation of the electronic structure of (super-) conducting or magnetic materials, the requirements are often much easier to meet since electronic spin effects combined with chemical or electronic inhomogeneity result in fast relaxing and/or broad NMR signals. On the other hand, for such materials the magnetic field is of importance also in another way: the external field can initiate sudden changes in the structure (e.g., electronic phase transitions) that are of great interest for the understanding of the properties of these materials and their applications (see e.g. [1,2]). One is therefore interested in applying magnetic fields of variable strengths, which, in addition, should reach the highest values possible. This interest in high magnetic fields is reflected by the tremendous efforts undertaken world wide by specialized high magnetic field laboratories that aim at supplying the highest magnetic fields [3].

While conventional superconducting magnets cease to operate much above 20 T, resistive magnets or hybrids of resistive and superconducting magnets are used to achieve higher fields of currently up to 45 T at the National High Magnetic Field Laboratory (Florida). Since resistive magnets need tremendous amounts of power that is dissipated in the conducting material it has to be perforated to allow for circulation of water for cooling purposes. This increases the size of the resistive magnets and makes them hardly usable at fields in excess of 35 T at which one needs a high-power (tens of Megawatts) grid connection, but also a cooling tower for the water. Up to now, the only way to reach much higher fields effectively consists in using pulsed magnets that were introduced by Kapitza [4] long ago (see also [5]). The idea is that the magnets are allowed to heat up during a short, intense field pulse and allowed to cool in-between pulses so that a rather compact coil design can be used that makes high fields possible. A low duty cycle for high magnetic field pulses keeps the average (dissipated) power low. The draw-back is that the high field is available only for a short time, and in addition, that it is intrinsically time-dependent.

Today, magnetic field pulses of up to 89 T have become available with such magnets [6] in non-destructive operation where the magnet can be used for a large number of such field pulses. Building magnets that can furnish such high magnetic fields for sufficient periods of time has become a challenge for engineering

* Corresponding author.
E-mail address: j.haase@physik.uni-leipzig.de (J. Haase).

1090-7807/$ - see front matter © 2011 Elsevier Inc. All rights reserved.
doi:10.1016/j.jmr.2011.02.007

since they have to sustain large changes in temperature from the power dissipation and high pressure from keeping the field confined in the magnet coil.

A new pulsed field facility, the Dresden High Magnetic Field Laboratory (*Hochfeld-Magnetlabor Dresden*, HLD), was built at the Forschungszentrum Dresden-Rossendorf in recent years [7]. In a joint effort of the University of Leipzig and the HLD we began setting up NMR at the HLD in 2008. Prior to the construction of the HLD some of us began to investigate the feasibility of performing NMR in pulsed high field magnets at a pilot pulsed magnet laboratory at the IFW Dresden. The magnets at the IFW Dresden, while being able to generate fields of up to almost 60 T, were only based on a 1.0 MJ capacitor bank (the HLD runs on a 50 MJ capacitor bank). As a result, early measurements were restricted to rather small magnet coils (large spatial inhomogeneity, very small NMR probes) during rather short magnetic field pulses (of a few milliseconds duration, cf. Fig. 1). Nevertheless, it was documented in various publications, e.g. [8–11], that NMR could be observed in these pulsed magnetic fields at up to 2.4 GHz resonance frequency or 58 T with home-built spectrometers. However, during the short rise time of such field pulses only nuclear spin systems with comparably small spin-lattice relaxation times T_1 can build up substantial longitudinal magnetization before the field maximum is reached so that a high signal-to-noise ratio can be achieved (unless the sample can be pre-polarized in an auxiliary static magnetic field).

With the new pulsed magnets at the HLD operational, we began constructing a new spectrometer that will be described elsewhere [12] and that is partly operated by the HLD control computers. Since the available energy is 50 times larger than what was available previously, larger coils with more space for probe heads and much longer field pulses make the HLD much more amenable to NMR experiments, cf. Fig. 1.

With our first set of experiments presented here we address the most notorious question, that of the temporal stability of the magnetic field. First, we show NMR signals at fields of up to 62 T (somewhat in excess of what has been reported so far [8]). Second, we show that we can excite and observe a large number of FIDs during a single magnetic field pulse. Third, we use the initial phases of all FIDs and their time evolution that are both influenced by the field's time dependence to actually fit $B(t)$ to a quadratic or cubic equation in time and find unprecedented precision, that, finally, allows us to demodulate and phase-correct the whole set of phase-locked FIDs. This enables us to perform signal averaging during a single magnet pulse as if the field were constant and stable.

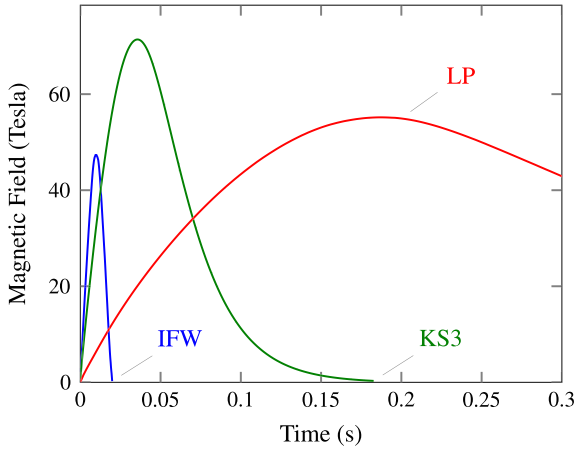

Fig. 1. Typical time dependencies of the magnetic field (low-resolution) achievable with three different magnet coils: IFW, at the IFW Dresden; KS3 and LP at the HLD. While fields above 60 T can only be generated with the KS3 coil, the LP coil offers a very long pulse duration and thus a much larger time slot for the acquisition of NMR signals.

2. Experimental

The HLD is described in detail elsewhere [13]. A large capacitor bank that can store up to 50 MJ of energy is at the heart of the laboratory. Various safe experimenter cells with home-built magnet coils are located around the capacitor bank. In a central control room a particular cell and the energy it receives is chosen by operating the corresponding electronic switches that load the capacitor bank from the grid and connect it with a particular cell's magnet coil. The triggered discharge leads to an almost sinusoidal current that builds up the magnetic field in the magnet coil. The dissipated heat is taken up by the magnet coil that sits in a bath of liquid nitrogen to whose temperature it returns slowly after the magnet pulse. The magnet coils in the various cells are designed for particular field profiles that may aim at the highest magnetic field and/or the longest duration of the field. They have outer diameters of about 250–650 mm with inner bores between 20 and 40 mm and typical lengths between 250 and 700 mm. Two typical time dependencies of the magnetic field $B(t)$ (low resolution) are shown in Fig. 1 together with a trace that was available at the IFW Dresden. Routinely performed measurements in these magnets concern resistivity [14,15], magnetization [16], ultrasound properties [17], as well as electron spin resonance (ESR) absorption [18].

For our NMR experiments, after the first search procedures with a small magnet coil A (time dependence of the field similar to that used at the IFW Dresden previously), we mainly used two different magnet coils that are labeled KS3 and LP for internal use at the HLD. The inner diameter of the cryostats that fit these magnet coils allowed the use of NMR probes with an outer diameter of about 16 and 32 mm for the KS3 and LP magnets, respectively (much larger than the 6 mm for the magnets at the IFW Dresden). The NMR probe consists of a 10 mm glass fiber reinforced plastic rod that carries a semi-rigid coaxial cable (EZ141 by Huber+Suhner, $Z = 50(1)$ Ohm). The probe fits in the cryostats that reach into the magnet coils and allow one to vary the probe temperature between about 4 and 300 K. The NMR probe head carries a resonance circuit with a cylindrical RF coil (typically 5–8 turns, 0.5 mm diameter copper wire) of about 3 mm length and 1 mm diameter and a ceramic chip capacitor of 1–10 pF. The circuit is matched to the coaxial cable by tapping the coil. This ensures a stable matching that is not much affected by closing the probe head with a cylindrical slitted aluminum cap. Note that fine tuning of the RF circuit is not necessary since the magnetic field pulse can be chosen by the charging voltage of the capacitor bank. The circuit's unloaded Q was typically about 40. A Pt-100 thermometer and two non-magnetic heating resistors of 8 Ohm were used to monitor and set the temperature of the sample.

Our new, home-built spectrometer (together with the probe) will be described in more detail elsewhere [12]. It is connected via Ethernet to the main computer that controls the capacitor bank. The actual resonance frequency of the probe while in the magnet coil and loaded with the sample is used to estimate the charging voltage of the capacitor-bank modules used. After charging is completed, a trigger pulse from the control room initiates the magnetic field pulse. A delay derived from this trigger pulse operates the spectrometer that initiates a series of constant frequency, in-phase RF pulses that are sent to the probe via the high-power RF amplifier (about 500 W). The receiver is locked to the same RF source the pulses are derived from and gated on after a dead-time delay of typically 3 μs after each RF pulse, and gated off shortly before each following RF pulse. Some time after the last RF pulse it is turned off

and the digital trace of FIDs is read out and processed as described further below.

For the experiment at low field (7.7 T) we used a solution of H_2O (2.5 ml) with $GdCl_3$ (52 mg) so that the ^1H spin lattice relaxation time as measured in static field was about 0.7 ms. For the experiment at high field (62 T) we used D_2O (2 ml) with 1 g of $GdCl_3$ giving a ^2H T_1 of 0.5 ms [19]. The solution was filled into a glass capillary of 1 mm diameter, which was sealed with glue and inserted into the RF coil.

Our very first experiments aimed at testing the spectrometer, in particular in connection with the control computer of the capacitor bank, and searching for test resonances (experiments on ^1H and ^{63}Cu NMR at up to 33 T with a small magnet coil were performed on a metal organic framework material and Cu metal, respectively). After the completion of those experiments we moved to another magnet with a new, much larger magnet coil (magnet LP) that had been built for long pulses, cf. Fig. 1. We started again searching for the ^1H NMR at low fields, which means small amounts of energy are deposited per field pulse in the magnet coil so that various pulses can be initiated before a substantial heating occurs. Once the resonances were found we were able to predict the maximum field based on the capacitor bank's charging voltage with a high enough accuracy (about 0.5%) to reliably observe NMR signals during every field pulse, and we began a more detailed study of the field's time dependence also at higher fields. Later, we moved to the magnet coil KS3 where the same procedure for measuring $B(t)$ was repeated up to the maximum field strength of 62 T.

3. Results and discussion

First, we report our results obtained at rather low pulsed field, slightly above 7.7 T. A train of 25 identical, equidistant (delay 1 ms) RF pulses (duration $\tau = 0.3$ μs) was derived from a single, stable RF carrier source running at a chosen frequency ω_0. The 25 excited FIDs of the ^1H magnetization of the liquid test sample ($T_1 \sim 0.7$ ms) were recorded in-between the RF pulses (see Experimental). After the experiment the receiver trace was dissected at times $t = t_j$, where t_j marks the begin of turning on the receiver after the jth RF pulse, cf. Fig. 2. The resulting set of 25 FIDs was Fourier transformed and the magnitude spectra are plotted as a function of

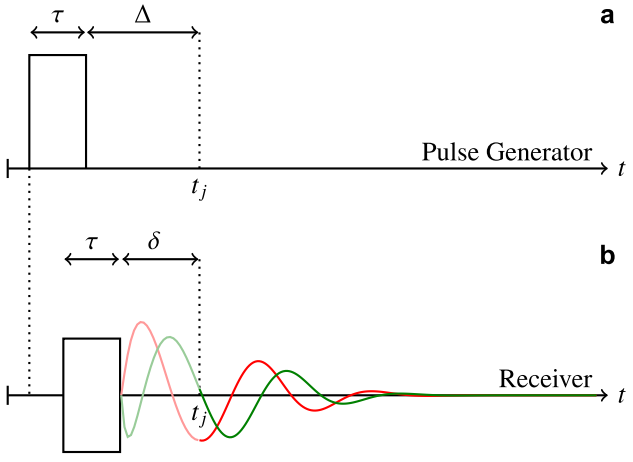

Fig. 2. Timing variables used in this paper. (a) τ, Δ, t_j are defined within the software that controls the pulse generator. After the jth RF pulse of duration τ we wait the dead-time $\Delta = 3$ μs before the receiver is turned on. (b) Due to delays during transmission and receiving of the FIDs the pulse and the signal appear shifted in time so that the effective dead-time is now $\delta < \Delta$. The red and green curve are a sketch of the NMR signal (IQ data). (For interpretation of the references to colour in this figure legend, the reader is referred to the web version of this article.)

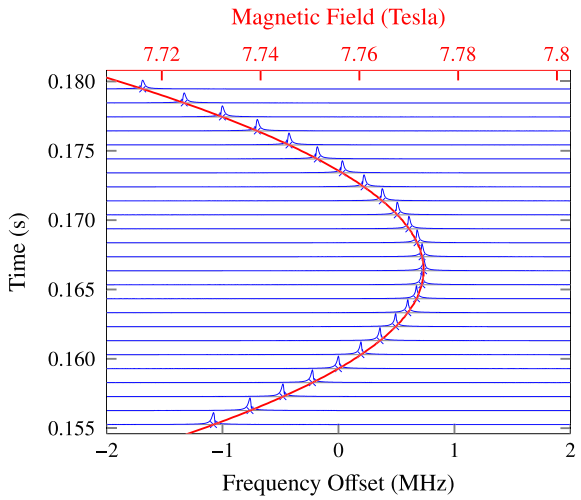

Fig. 3. Magnitude Fourier transform spectra of all 25 FIDs vertically offset by the time when acquisition started. The crosses show a projection of the maxima to the baseline of a given spectrum. With the carrier frequency at about 330 MHz each maximum is interpreted as a measure of B at time t_j. The full line shows a fit of the maxima of the spectra to $B_{\mathrm{fit}}(t)$ from Eq. (1), see text.

the time $t = t_j$ in Fig. 3. As the 2nd axis we show in Fig. 3 the frequency or resonance offset $\Delta\omega = \omega - \omega_0$. One notices from Fig. 3 that we were able to record spectra with similar intensities after each RF pulse over the entire time interval of about 25 ms during which the magnetic field varied continuously. Also shown in Fig. 3 (full red line) is $B_{\mathrm{fit}}(t)$ as determined from the maxima of the spectra in the following way. We describe $B(t)$ with a minimal set of parameters in the vicinity of its maximum ($t \sim t_{\max}$) where we expect a quadratic or cubic dependence on time to hold. We therefore write,

$$B_{\mathrm{fit}}(t) = B_{\max}\left(1 - \alpha(t - t_{\max})^2 + \beta(t - t_{\max})^3\right), \tag{1}$$

where α and β are positive constants, and $B_{\max}$ is the field maximum that occurs at $t = t_{\max}$.

A nonlinear least-squares fit is performed using Matlab's implementation of the Levenberg-Marquardt algorithm in order to obtain $B_{\max}$, $t_{\max}$, α and β from the maxima of the magnitude spectra. The algorithm returns the coefficient estimates, the residuals, the Jacobian and a covariance matrix for the fitted coefficients. For each parameter the 95% confidence interval as specified in Table 1 is obtained as $a \pm ts$ where t is derived from Student's t Distribution using the degrees of freedom and the required confidence and s denotes the standard error, i.e. the square root of the given diagonal entry of the covariance matrix. The obtained values are shown in the first row of Table 1.

Clearly, using the maxima of the (not demodulated) magnitude spectra for the determination of $B(t)$ will give us not more than rough estimates for the parameters in (1), and we take them only as the starting values in a more rigorous analysis that will be described now.

We note that the detection yields a set of $j = 1, \ldots, N$ complex valued (I/Q) FIDs $G_{\exp,j}(t) = I_j(t) + iQ_j(t)$. We can think of each individual FID as

$$G_j(t) = G_{0,j}e^{-(t-t_j)/T_2}e^{+i\phi_j(t)}. \tag{2}$$

The initial amplitude $G_{0,j}$ is given by the jth RF pulse (including the probe properties), and the longitudinal magnetization before the pulse (the dependence on the actual frequency $\omega_j = \gamma B(t_j)$ can be neglected). The observed amplitudes of the FIDs are within the limits of what we expect based on the number of resonant

Table 1
Results from fitting the maxima of the magnitude spectra, 1st and 3rd row, to Eq. (1), and fitting the experimental time evolution of the phase, 2nd and 4th row, to Eq. (3) by varying the parameters of Eq. (1). The experiments with the LP and KS3 magnet were performed at about 7.77 and 62.2 T, respectively. The change of $B(t)$ during each FID is not taken into account by the Fourier transform fitting procedure leading to systematic deviations of α and β from there values as obtained by the phase fitting procedure.

Coil	Fit	B_{max} (T)	t_{max} (s)	α (s^{-2})	β (s^{-3})	δ (μs)	ϕ_0 (rad)
LP	FT	7.773012(9)	0.166403(3)	43.54(2)	46(2)	–	–
LP	ϕ	7.7729823(2)	0.16644153(6)	43.5710(4)	41.88(6)	2.15	1.66
KS3	FT	62.164(1)	0.048446(4)	91(5)	–	–	–
KS3	ϕ	62.16467(5)	0.0484605(2)	91.6(2)	–	2.15	−0.79

nuclei in the sample [12]. The apparent decay time of ∼30 μs is shorter than what one estimates from the measured T_1 of 0.7 ms. The FIDs far away from $t = t_{max}$ are dominated by a modulated phase from the strong time dependence of the field. Near the field maximum, however, the decays remained rather short probably due to the inhomogeneity of the field across our small samples. Preliminary spin-echo experiments showed no decay of the echo amplitudes out to at least 100 μs pulse separation pointing indeed to inhomogeneous broadening. Note, that the maximum field cannot be predicted from one field pulse to another with a high accuracy, and together with the low repetition of field pulses, the investigation of the field distribution as a function of probe position is a lengthy task. Nevertheless, experiments are under way to investigate the magnets used here in more detail with special probe designs. Here, we focus on the time dependence of the magnetic field, that also contributes to the linewidths due to the modulation of the signal's average phase.

Note, that since all RF pulses in the train are derived from the same carrier (ω_0) to which also the receiver is locked, the (time-dependent) phase $\phi_j(t)$ of the jth FID in the rotating frame (ω_0) can be written as, cf. Fig. 2,

$$\phi_j(t) = \phi_0 + \phi_{\tau,j} + \int_{t_j-\delta}^{t} [\gamma B(t') - \omega_0]dt'. \tag{3}$$

Here, ϕ_0 is a fixed phase difference between transmitter and receiver. The second term describes the action of the very short RF pulse during which we can assume the field to be constant ($B(t) = B(t_j)$). $\phi_{\tau,j}$ follows from an effective Hamiltonian $\mathscr{H}_{\tau,j} = \hbar\Delta\omega_j I_z + \hbar\omega_{RF} I_x$, where $\Delta\omega_j = \omega_j - \omega_0$ denotes the resonance offset and ω_{RF} the RF pulse amplitude. For the evolution of the phase after the RF pulse the time-dependent field occurs in the integral.

Note that the time t_j has only a precise meaning within the pulse-generation sequence as it does not include phase changes during transmitting and receiving, cf. Fig. 2. At a given carrier frequency (ω_0), this difference in time is set by the hardware and gives rise to the phase difference ϕ_0 in (3). However, since each FID $G_j(t)$ in (2) has a varying frequency offset, it will acquire another phase difference during the time interval δ between the end of the pulse and t_j, cf. Fig. 2. This phase lag is taken into account by using $t_j - \delta$ as the lower bound for the integral in (3).

From our experimental data $G_{exp,j}(t) = I_j(t) + iQ_j(t)$ we have the phase of each FID as well as its evolution with time. Note that the phase is well defined only for a sufficiently large signal-to-noise ratio, that is why we use from the FIDs only about the first 150 μs where the amplitude is clearly above the noise. Now that we have a set of experimental phases $\phi_{exp,j}(t)$ we use again (1) with the parameters determined earlier as starting values for fitting $\phi_j(t)$ to $\phi_{exp,j}(t)$ using the same algorithm as described above. We used a $\pi/2$ pulse and varied ϕ_0 and δ manually minimizing the deviation of $\phi_j(t_j)$ from $\phi_{exp,j}(t_j)$, see Table 1. As one might expect, this fitting protocol results in more accurate estimates of the coefficients in (1), the main result being a decrease of the error in B_{max} down to 0.03 ppm. Confer the second row of Table 1 for all estimates. Such a high precision suggests that we can use (1) with the parameters from Table 1 and demodulate and phase-correct all FIDs at once.

We note that we can use (3) in order to remove the effect of the time-dependent resonance frequency from $\phi_{exp,j}(t)$ and the thus transformed FIDs should all be identical (no dependence on j), i.e.,

$$\widetilde{G}_{exp}(t) = G_{exp,j}(t)\exp\left(-i\phi_j(t)\right). \tag{4}$$

In order to plot the FIDs as a function of the field's deviation from $B(t_j)$ we simply modify our experimentally obtained FIDs according to

$$\widetilde{G}_{exp,j}(t) = G_{exp,j}(t)\exp\left(-i\phi_j(t_j) - i\gamma\int_{t_j}^{t}\left[B(t') - B(t_j)\right]dt'\right). \tag{5}$$

The real parts of the Fourier transforms following from (5) (with an additional 5 kHz exponential line broadening) are displayed in Fig. 4. All frequency-modulations have disappeared, the linewidths are the same and the spectra appear to be almost perfectly phase-locked. In fact, the slight discrepancy in the phase of the last five spectra is accompanied by a loss in intensity, indicating that the effective flip-angle had changed (we believe this is due to heating of the probe after all the pulses).

Also shown in Fig. 4, the blue spectrum to the far left, is the real part of the Fourier transform of the sum of all signals divided by the factor $N = 25$, i.e., the Fourier transform of

$$\widetilde{G}_{exp}(t) = \frac{1}{N}\sum_{j=1}^{N} G_{exp,j}(t)\exp\left(-i\phi_j(t)\right). \tag{6}$$

Obviously, this spectrum is very similar to the individual ones and has nearly the same intensity. We find an increase in the experimental signal-to-noise ratio of 4.7, close to the theoretical value of $\sqrt{25}$.

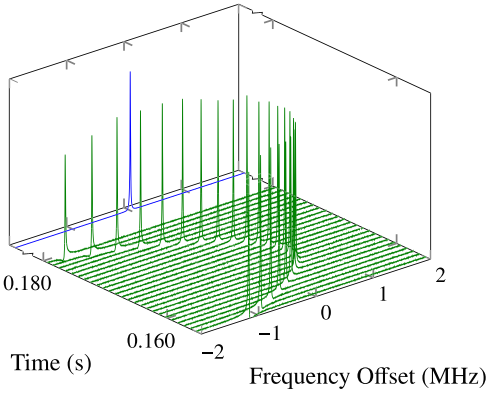

Fig. 4. 7.77 T experiment; real parts (green lines) of Fourier transform spectra of the 25 FIDs demodulated using (5) plotted as a function of the time t_j. Note that the adjustable phase ϕ_0 in (3) is the same for all spectra. The blue line shows the real part of the averaged spectrum, i.e. the Fourier transform of (6). (For interpretation of the references to colour in this figure legend, the reader is referred to the web version of this article.)

We think these are very encouraging results. While it was shown earlier that a single FID could be demodulated successfully at low pulsed-field strength [20], we here demodulate *and* phase-correct a set of 25 FIDs with two adjustable parameters ϕ_0 and δ. This means that by monitoring the field with a reference sample one can obtain highly precise knowledge of the field over a large period of time and one is able to predict all initial signal phases. By simultaneously measuring a 2nd signal (with a double-resonance probe) one could perform signal averaging and shift measurements with high precision. In essence, the presented results show that one can remove the time dependence of the field so that all signals appear to be taken in a magnet at a stable, constant field.

Now, the obvious question arises whether such a procedure also works at much higher fields that cannot be reached with ordinary magnets. In addition, it would be interesting to see whether one can obtain such a result also with other magnet coils. We, therefore, performed similar analyses at 43 T with magnet LP and 62 T with magnet KS3. We found in deed similar results and describe one experiment at 62 T in more detail below.

Here, a train of 10 RF pulses ($\tau = 0.5$ µs, delay 0.5 ms) derived from the RF carrier running at about 400 MHz was used to excite ^{2}H NMR FIDs of a D_2O sample in magnet KS3 (see Experimental). The signals were recorded in-between pulses and the receiver trace was again dissected at times t_j as described earlier. The magnitude spectra, presented similar to Fig. 3, can be found in Fig. 5.

The spectra taken on the steeper slope of the field, i.e., away from the field maximum, clearly show modulation features from the time-dependent field during signal decay (note that the duration of the field pulse in magnet KS3 is shorter, cf. Fig. 1, so that the modulation is easier to see in comparison to Fig. 3). We also observe a somewhat stronger variation of the signal intensities in Fig. 5 compared to Fig. 3. This is probably caused by the limited bandwidth of the probe. The overall lower signal-to-noise ratio is due to a smaller number of ^{2}H in the sample. Also shown in Fig. 5 is $B(t)$ as derived from the peak frequencies of the magnitude spectra and their fit to the magnetic field time dependence according to (1). The fitted parameters are displayed in Table 1 (note that the cubic term is absent, i.e. $\beta = 0$, since we are relatively closer to the field maximum).

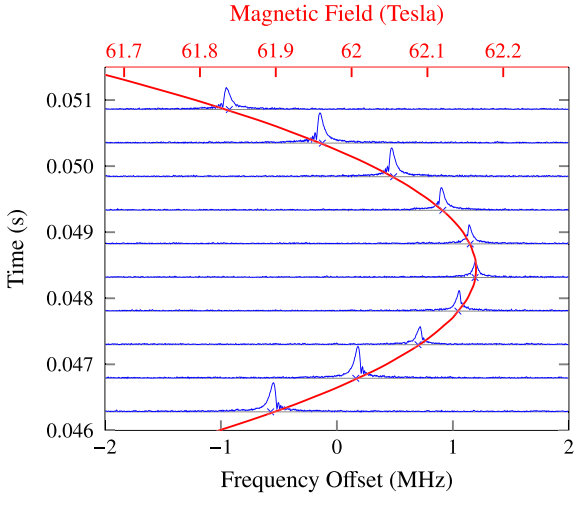

Fig. 5. Magnitude Fourier transform spectra of all 10 ^{2}H FIDs obtained during a single field pulse in the KS3 magnet at 62 T vertically offset by the time when acquisition started. The crosses show a projection of the maxima to the baseline of a given spectrum. Due to the stronger time dependence frequency-modulation effects are clearly visible in the spectra away from the field maximum. The full red line shows a fit of the maxima of the spectra to $B_{fit}(t)$ from Eq. (1), see text. (For interpretation of the references to colour in this figure legend, the reader is referred to the web version of this article.)

From our 10 experimental FIDs $G_{exp,j}(t)$ we again calculate a set of experimental phases $\phi_{exp,j}(t)$ and their evolution with time. We then use the just described parameters that are displayed in the 3rd row of Table 1 and fit $\phi_j(t)$ from (3) to $\phi_{exp,j}(t)$ by varying the parameters of (1) in order to obtain new values for the parameters that describe the time dependence of the field more accurately. They are presented in the 4th row of Table 1. Also shown is the manually fitted overall phase ϕ_0 and dead-time δ (in fact, since there was no time to measure the flip-angle of the pulse precisely at such high field, we determined it with the fit, as well, and found 2.1 rad instead of the estimated 1.57). Remarkably, the precision of the fit to the magnetic field is very good, albeit quite a bit less good when compared to that at low field where 25 FIDs were available. Since probe and spectrometer hardware remained essentially the same when moving over to the KS3 magnet (only a small difference in frequency), we are not surprised to find the same dead-time δ with a somewhat different total phase ϕ_0.

In a next step, we use the thus determined $B_{fit}(t)$ and demodulate and phase-correct the experimental FIDs $G_{exp,j}(t)$ according to (5). The result, the real parts of the Fourier transforms of the individual spectra (additional exponential broadening of 10 kHz) as a function of field are displayed in Fig. 6 (green lines), together with the sum of the real parts of the Fourier transforms (same additional broadening) of the FIDs demodulated according to (4) divided by the factor 10 (blue spectrum to the far left). The improvement in the signal-to-noise ratio is 3.0 and close to what we expect from averaging 10 FIDs. This shows that the procedure of demodulating and phase-correcting works also well at high fields. The knowledge of the field after the experiment is rather precise so that simultaneous shift measurements on an unknown sample should be possible.

We think that we could prove that the time dependence of the field in the investigated pulsed magnets does not pose a serious problem for NMR measurements (at the HLD). While it is, e.g., not possible to predict with the necessary accuracy neither the point in time of the occurrence of the field maximum nor its amplitude with sufficient accuracy before the experiment, after the experiment, we know the field with very high precision over a large period of time. Variations in the charging voltage of the capacitor bank (that always has a slight power leakage), small differences in the magnet base temperature, and perhaps a range of other factors seem to prevent us from improving sufficiently on the prediction of the actual field such that we can reach chemical-shift precision. On the other hand, the knowledge of the field

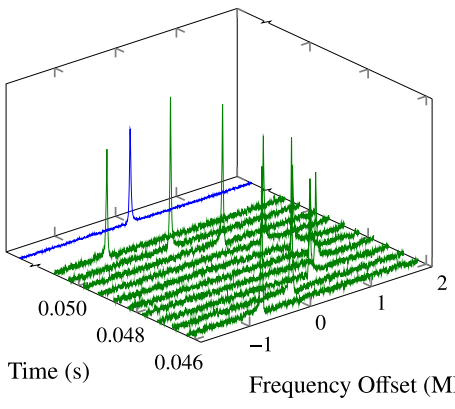

Fig. 6. 62 T experiment; real parts (green lines) of Fourier transform spectra of the 10 FIDs demodulated using (5) plotted as a function of the time t_j. Note that the adjustable phase ϕ_0 in (3) is the same for all spectra. The blue line is again the real part of the averaged spectrum, i.e. the Fourier transform of (6). The improvement in the signal-to-noise ratio is clearly visible. (For interpretation of the references to colour in this figure legend, the reader is referred to the web version of this article.)

obtained after the field pulse seems to be limited only indirectly by the homogeneity of the field across the sample, at least at the current level of already very high accuracy.

Clearly, while we can approach NMR experiments on real samples already, the homogeneity of the magnetic field has to be investigated. Now, we can remove most of the broadening from the field's time dependence for FIDs taken away from the field maximum, which always occurs since the maximum of the field cannot be predicted with high enough accuracy at high fields. For the experiments shown, after the demodulation, we find linewidths of 8–12 kHz for the real parts of the spectra for ^{1}H at 7.8 T in the LP magnet and 16–21 kHz for ^{2}H at 62 T in the KS3 magnet. We assume that it is possible to improve the resolution significantly. Another set of experiments concerns the use of a double-resonance probe with two samples. Here, one test sample measures the magnetic field as demonstrated above while the other measures an unknown shift.

Acknowledgments

This work was supported by Deutsche Forschungsgemeinschaft within the Graduate School BuildMoNa and ESF project no. 080935191. Part of this work was supported by EuroMagnet II, EU contract no. 228043. B.M., J.H. would like to thank S. Berger (University of Leipzig), M.S. Conradi (Washington University, St. Louis) for helpful discussions, as well as M. Bartkowiak (HLD), M. Bertmer, D. Freude, D. Rybicki, H. Voigt (University of Leipzig).

References

[1] S.-i. Tani, H. Inoue, T. Suzuki, S. Hosoya, K. Inokuchi, T. Fujiwara, T. Goto, H. Tanaka, T. Sasaki, S. Awaji, K. Watanabe, N. Kobayashi, Cu-NMR study on field-induced phase transitions in quantum spin magnet NH_4CuCl_3, Prog. Theor. Phys. Suppl. 159 (2005) 235–240.

[2] S. Kawasaki, C. Lin, P.L. Kuhns, A.P. Reyes, G.-q. Zheng, Carrier-concentration dependence of the pseudogap ground state of superconducting $Bi_2Sr_{2-x}La_xCuO_{6+\delta}$ revealed by ^{63,65}Cu-nuclear magnetic resonance in very high magnetic fields, Phys. Rev. Lett. 105 (2010).

[3] T. Herrmannnsdörfer, F. Wolff-Fabris, in: Proceedings of the 2009 international conference on research at high magnetic fields RHMF (2009), Journal of Low Temperature Physics, 159, 2010.

[4] P.L. Kapitza, A method of producing strong magnetic fields, Proc. R. Soc. A 105 (1924) 691–710.

[5] F. Herlach, N. Miura, High Magnetic Fields: Science and Technology: Magnet Technology and Experimental Techniques, World Scientific Publishing Company, 2003.

[6] J.R. Sims, D.G. Rickel, C.A. Swenson, J.B. Schillig, G.W. Ellis, C.N. Ammerman, Assembly, commissioning and operation of the NHMFL 100 Tesla multi-pulse magnet system, IEEE Trans. Appl. Supercond. 18 (2008) 587.

[7] J. Wosnitza, A. Bianchi, J. Freudenberger, J. Haase, T. Herrmannsdörfer, N. Kozlova, L. Schultz, Y. Skourski, S. Zherlitsyn, S. Zvyagin, Dresden pulsed magnetic field facility, J. Magn. Magn. Mater. 310 (2007) 2728–2730.

[8] J. Haase, First ^{2}H NMR at 58 T, Appl. Magn. Reson. 27 (2004) 297–302.

[9] J. Haase, D. Eckert, H. Siegel, H. Eschrig, K.H. Müller, F. Steglich, High-field NMR in pulsed magnets, Solid State Nucl. Magn. Reson. 23 (2003) 263–265.

[10] J. Haase, M. Kozlov, K. Müller, H. Siegel, B. Büchner, H. Eschrig, A. Webb, NMR in pulsed high magnetic fields at 1.3 GHz, J. Magn. Magn. Mater. 290–291 (2005) 438–441.

[11] G.-q. Zheng, K. Katayama, M. Nishiyama, S. Kawasaki, N. Nishihagi, S. Kimura, M. Hagiwara, K. Kindo, Spin–Echo NMR in pulsed high magnetic fields up to 48 T, J. Phys. Soc. Jpn. 78 (2009) 095001.

[12] B. Meier, J. Haase, M. Braun, F. Wolff-Fabris, T. Herrmannsdörfer, J. Wosnitza, in preparation.

[13] J. Wosnitza, T. Herrmannsdörfer, Y. Skourski, S. Zherlitsyn, S.A. Zvyagin, O. Drachenko, H. Schneider, M. Helm, A. Ghoshray, B. Bandyopadhyay, Science at the Dresden high magnetic field laboratory, AIP Conf. Proc. 1003 (2008) 311–315.

[14] T. Helm, M.V. Kartsovnik, M. Bartkowiak, N. Bittner, M. Lambacher, A. Erb, J. Wosnitza, R. Gross, Evolution of the fermi surface of the Electron-Doped High-Temperature superconductor $Nd_{2-x}Ce_xCuO_4$ revealed by Shubnikov-de Haas oscillations, Phys. Rev. Lett. 103 (2009) 157002.

[15] T. Helm, M.V. Kartsovnik, I. Sheikin, M. Bartkowiak, F. Wolff-Fabris, N. Bittner, W. Biberacher, M. Lambacher, A. Erb, J. Wosnitza, R. Gross, Magnetic breakdown in the electron-doped cuprate superconductor $Nd_{2-x}Ce_xCuO_4$: the reconstructed Fermi surface survives in the strongly overdoped regime, Phys. Rev. Lett. (2010).

[16] A.V. Andreev, M.D. Kuz'min, Y. Narumi, Y. Skourski, N.V. Kudrevatykh, K. Kindo, F.R. de Boer, J. Wosnitza, High-field magnetization study of a Tm_2Co_{17} single crystal, Phys. Rev. B 81 (2010).

[17] A. Sytcheva, U. Löw, S. Yasin, J. Wosnitza, S. Zherlitsyn, T. Goto, P. Wyder, B. Lüthi, Magneto-acoustic Faraday effect in $Tb_3Ga_5O_{12}$, J. Low Temp. Phys. 159 (2010) 126–129.

[18] S.A. Zvyagin, M. Ozerov, E. Čižmár, D. Kamenskyi, S. Zherlitsyn, T. Herrmannsdörfer, J. Wosnitza, R. Wünsch, W. Seidel, Terahertz-range free-electron laser electron spin resonance spectroscopy: Techniques and applications in high magnetic fields, Rev. Sci. Instrum. 80 (2009) 073102.

[19] N. Bloembergen, E.M. Purcell, R.V. Pound, Relaxation effects in nuclear magnetic resonance absorption, Phys. Rev. 73 (1948) 679.

[20] J. Haase, D. Eckert, H. Siegel, H. Eschrig, K. Müller, A. Simon, F. Steglich, NMR at the frontier of pulsed high field magnets, Physica B 346-347 (2004) 514–518.